ACCEPTED MANUSCRIPT

Study of turbulence modulation and core density peaking with CO₂ laser collective scattering diagnostics in EAST tokamak

To cite this article before publication: Pan Li *et al* 2020 *Nucl. Fusion* in press https://doi.org/10.1088/1741-4326/ab796c

IOP Publishing Journal Title
Journal **XX** (XXXX) XXXXXX https://doi.org/XXXX/XXXX

Study of turbulence modulation and core density peaking with CO_2 laser collective scattering diagnostics in EAST tokamak

P. Li[1,2,a], Y. D. Li[2,a], J. G. Li[2], G. J. Wu[2], T. Lan[1], B. Zhang[3], J. S. Geng[2], Y. K. Zhang[2], L. Q. Xu[2], H. L. Wang[2] and H. Q. Liu[2]

[1]University of Science and Technology of China, Hefei 230026, People's Republic of China;

[2]Institute of Plasma Physics, Chinese Academy of Sciences, Hefei 230031, People's Republic of China;

[3]East China University of Technology, Nanchang 330013, People's Republic of China;

E-mail: yd_li@ipp.ac.cn and lipan@ipp.ac.cn

Abstract

Progress from experiment in understanding the interaction between electron-scale turbulence and plasma poloidal flow in tokamak is reported. Multiple electron-scale turbulence (for $0.8 \leq k_\theta \rho_s \leq 4$) in plasma radial region ($\rho = 0 - 0.8$) is simultaneously monitored by CO_2 laser collective scattering diagnostics in EAST tokamak. In stable discharge phase with ECRH power modulation and constant NBI injection, a periodically change of core density peaking factor ($\langle n_e(0)\rangle / \langle n_e(0.5)\rangle$) can be obtained. We note that the intensity of turbulence and core density peaking factor show a negative correlation, while the poloidal rotation speed is inversely proportional to the intensity of electron-scale turbulence. The correlation between turbulence and plasma flow are found closely related to the density peaking factor. The quasi-linear theory of electron-scale turbulence driven intrinsic poloidal rotation is adopted, and it shows that plasma flow may exhaust the free energy of turbulence through Reynolds stress. Besides, by comparing the plasma flow shear and spatial cross-correlation of turbulence, we observed that the spatial structure of turbulence at $k_\theta = 12\ cm^{-1}$ is more sensitive to flow shear than that of turbulence at $k_\theta = 22\ cm^{-1}$. The possible mechanism for controlling the core density peaking ($\rho = 0 - 0.5$), together with unchanged density gradient in outer ($\rho = 0.5 - 0.8$), are favorable for controlling fusion reactions rate if they can be extrapolated to burning plasma. The results in ECRH power modulation experiments without NBI are listed and analyzed simultaneously, which serve as a comparison and enrich the physical picture.

Keywords: electron-scale turbulence, plasma flow, self-organizing, density peaking, tokamak

1. Introduction

Plasma density profile are directly related to the operation and the overall fusion gain. A burning plasma is fundamentally different from plasmas that have been created in all research facilities to date, due to the interpose is difficult to achieve in the core plasma and the highly self-organized plasma configuration. Fueling including pellet ablation and edge neutral gas ionization in ITER-like fusion reactor occur outside the pedestal zone and pedestal zone [1]. Non-diffusive transport in the core plasma will be a key factor.

Fusion performance increases with density. The collisionality dependence of density peaking in JET implies a physics mechanism of anomalous particle transport, which may help dispel the concern of density limit [2]. The nature of the turbulence is usually link to density peaking in experiments [3]. And the mechanism is simulated with a fluid model of drift wave turbulence [4], in which particle transport caused by turbulence is regime dependent [5]. The thermo-diffusive pinch included by ion temperature gradient modes (ITGs) is inward while the direction is inversed in

[a] Authors to whom any correspondence should be addressed.

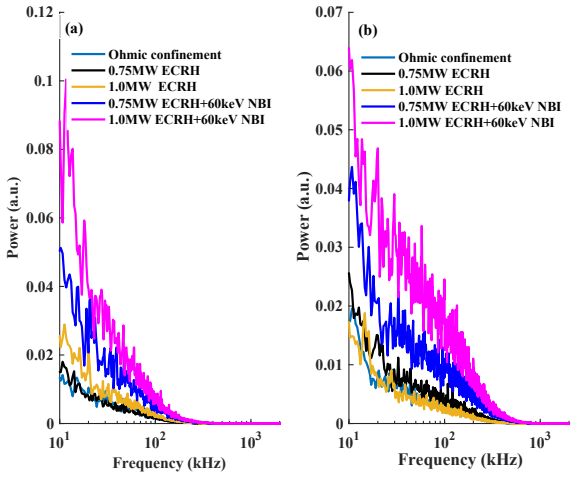

Figure 1. The power spectrum of turbulence in core (a) k = 12cm^{-1}, (b) k = 22cm^{-1}. Data from shot 80742 and shot 80744 in EAST.

trapped electron modes (TEMs) regime. The peaked density profile can be well understood in terms of ITG+TEM driven transport [6,7,8], while density pumpout effect has been qualitatively explained by the presence of TEMs [9,10].

The turbulence intensity, turbulence spatial correlation and the transport cross phase can be affected by plasma flows, which is stabilizing for turbulent transport [11,12,13,14]. However, there is a free energy exchange process between turbulence and plasma flows via Reynolds stress [15,16]. Turbulence spectrum asymmetry and turbulence nonlinear dynamic is also considered to be the source of the residual Reynolds stress, which can drive zonal flow and/or mean flow [15,17,18]. And the intrinsic poloidal rotation will be the dominate team of $\mathbf{E} \times \mathbf{B}$ flow in future fusion reactor, because of the low injected torque. Theories of intrinsic rotation generated by electromagnetic turbulence [19] and electrostatic turbulence [11] have been studied respectively. Optimization of plasma performance need more work on the understanding these interactions in the plasma.

EAST is a toroidal tokamak operating with major radius R = 1.85m and minor radius a = 0.45m. Data in the paper are from reproducible EAST stable discharges with toroidal magnetic field $B_T = 2T$, the plasma current $I_P = 0.45MA$ and density $n_e = 1.9 - 3.3 \times 10^{19}\ m^{-3}$. The collision frequency (electron-ion) normalized to drift frequency $\nu_{eff} = \frac{\nu_{ei}}{\omega_{DE}} \approx 0.1 n_e Z_{eff} \frac{R}{T_{ek}^2}$ [20] is about 1.85 in the region $\rho = 0 - 0.4$. The non-Maxwellian electron velocity distribution changed by locally heated electrons can influence the free energy that driving electron-scale turbulence [21]. In this experiments the off-axis ECRH uses the second harmonic extraordinary (X2) mode at 140 GHz with two gyrotrons [22], one gyrotorn (EC1) is modulated at 0.25MW and 0.5MW with a frequency of 2 Hz and the other gyrotorn (EC3) is 0.5MW. The experiments with or without constant NBI are performed separately. Electron-scale turbulence is measured by CO_2 laser collective scattering diagnostics [23,24,25,26], which is introduced in section 2. The turbulence power spectrums under different auxiliary heating are shown in figure 1. With the same ECRH power modulation heating, the presence or absence of NBI injection has a different impact on the turbulence power spectrum, which may imply a internal difference.

This paper is organized as follows. Section 2 provides the descriptions of the CO_2 laser collective scattering diagnostics and the measurement techniques of turbulence and poloidal rotation velocity in EAST. In section 3, electron-scale turbulence and plasma flow in two shots with different conditions are presented. And the possible mechanism of density peaking factor modulation is presented experimentally. In section 4, turbulent-driven quasilinear theory quantitative analysis the possible correlation of turbulence gradient and plasma flow, and the possible influences of plasma flow shear on the spatial cross-correlation of multiple electron-scale turbulence are also analyzed. Section 5 discusses the core density peaking factor in the presence of sawteeth. Finally, the main conclusions and disadvantages of this work are shown in section 6.

2. Experimental Techniques and Apparatus

The CO_2 laser collective scattering diagnostics in EAST is based on the collective scattering principle [24]. The diagnostics is shown schematically in figure 2. The single mode TEM_{00} laser $(\omega_0, \vec{k}_0)$ has a beam waist radius of 1 cm and a frequency of 28 THz. This frequency is much larger than that of the electron plasma 10^{-2} THz, and the effects of refraction and diffraction can be ignored [24,26].

The wave vectors of microturbulence at the electronic scale are mainly perpendicular to the magnetic field $(\mathbf{k} \cdot \mathbf{B} \approx 0)$. Covering the optical path of the probe light passing through the plasma, two scattering planes are constructed at 85° and 90° to the magnetic axis, respectively. In each scattering plane, two local oscillator (LO) beams $(\omega_{LO}, \vec{k}_{LO})$ intersect the probe beam in a region at two different angles θ. The drift wave turbulence $(\omega, \vec{k})$ and the scattered wave $(\omega_s, \vec{k}_s)$ satisfy energy and momentum conservation requirements so that

$$\vec{k}_s = \vec{k}_0 \pm \vec{k} \text{ and } \omega_s = \omega_0 \pm \omega \quad (1)$$

Co-directional scattered electromagnetic wave from the probe light in the intersecting volume will be mixed with the LO beam $(\omega_{LO}, \vec{k}_{LO})$ and enter the $H_gC_dT_e$ detector finally. The intensity of the photoelectric signal received by the detector is

$$\begin{aligned} i_s \propto |E(t)|^2 &= |A_s \cos(\omega_s t + \varphi_s) + A_{LO} \cos(\omega_{LO} t + \varphi_{LO})|^2 \\ &= |A_s \cos(\omega_s t + \varphi_s)|^2 + |A_{LO} \cos(\omega_{LO} t + \varphi_{LO})|^2 \\ &\quad + |A_s A_{LO} \cos[(\omega_s + \omega_{LO})t + (\varphi_s + \varphi_{LO})]| \\ &\quad + |A_s A_{LO} \cos[(\omega_s - \omega_{LO})t + (\varphi_s - \varphi_{LO})]| \end{aligned} \quad (2)$$

The frequencies of the first three terms on the right side of

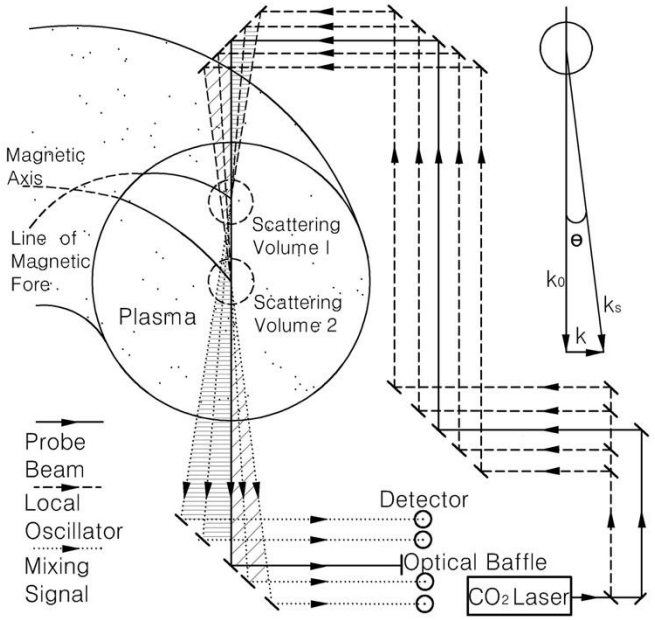

Figure 2. CO_2 laser collective scattering diagnostics.

the equation are outside the detector response range, which are output as a constant. The output photoelectric signal of the detector is

$$\mathrm{i} \propto |A_s A_{LO}| \cos[\omega t + (\varphi_s - \varphi_{LO})] \quad (3)$$

A_{LO} is a constant. For the team A_s, scattered power is proportional to the square of the density perturbation [26],

$$\mathrm{P}_s = \frac{1}{4} P_0 r_e^2 \lambda_i^2 \tilde{n}_e^2 L_V^2 \quad (4)$$

P_0 is probe beam power, $\mathrm{r_e}$ is the classical radius of electron, λ_i is the wavelength of probe beam, $\tilde{n}_e$ is the fluctuation of electron density, L_V is the length of scattering volume. Turbulence information and corresponding intensity can be obtained by Fourier decomposition of the obtained photoelectric signal. The measured **k** mainly contains the poloidal component $\boldsymbol{k_\theta}$ of turbulence and a very small radial component $\boldsymbol{k_r}$.

For the interested drift wave number, $\vec{\mathrm{k}}_0 \approx \vec{\mathrm{k}}_s$, the scattering angle $\theta < 0.3^\circ$ will satisfy Bragg relation, yielding

$$\mathrm{k} = 2\mathrm{k}_0 \sin(\theta/2) \quad (5)$$

We can determine the wave number of turbulence we need measure by adjusting the scattering angle. The spatial positions of the intersecting volumes of the LO beams and the probe beam in the two scattering planes are different, which determine the final detection regions.

In 2018, the multichannel scattering system covering two plasma regions (core $\rho = 0 - 0.4$, outer $\rho = 0.4 - 0.8$), and two wave numbers ($\mathrm{k}_\theta = 12\ \mathrm{cm}^{-1}$ and $\mathrm{k}_\theta = 22\ \mathrm{cm}^{-1}$, correspondingly $\mathrm{k}_\theta \rho_s \sim 0.8 - 4.0$ in the experiments) are measured simultaneously in each region [25]. It can monitor turbulent spatial structure in EAST, and research the turbulent characteristic. Figure 3 and figure 4 show the spectrograms of turbulence with wave numbers of $\mathrm{k}_\theta =$

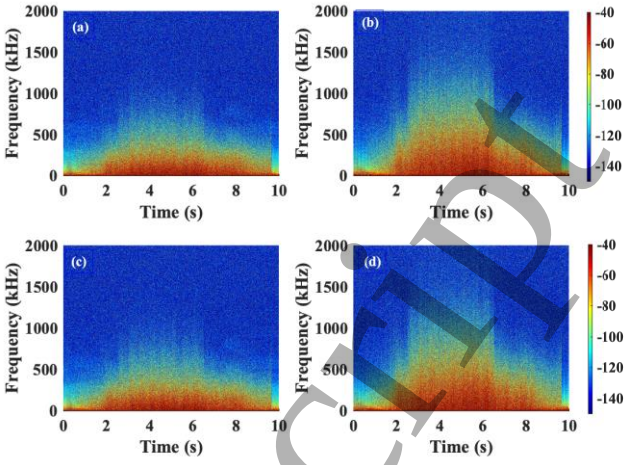

Figure 3. Shot 80744, time evolution of turbulent spectrograms. (a) $\mathrm{k} = 12\mathrm{cm}^{-1}$ in $\rho = 0 - 0.4$, (b) $\mathrm{k} = 22\mathrm{cm}^{-1}$ in $\rho = 0 - 0.4$, (c) $\mathrm{k} = 12\mathrm{cm}^{-1}$ in $\rho = 0.4 - 0.8$ and (d) $\mathrm{k} = 22\mathrm{cm}^{-1}$ in $\rho = 0.4 - 0.8$.

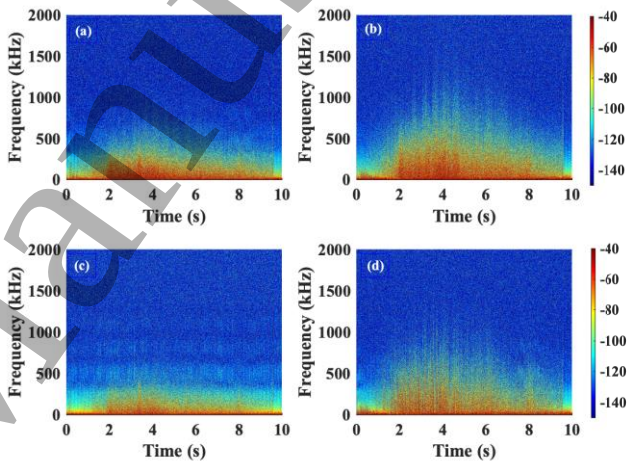

Figure 4. Shot 80742, time evolution of turbulent spectrograms. (a) $\mathrm{k} = 12\mathrm{cm}^{-1}$ in $\rho = 0 - 0.4$, (b) $\mathrm{k} = 22\mathrm{cm}^{-1}$ in $\rho = 0 - 0.4$, (c) $\mathrm{k} = 12\mathrm{cm}^{-1}$ in $\rho = 0.4 - 0.8$ and (d) $\mathrm{k} = 22\mathrm{cm}^{-1}$ in $\rho = 0.4 - 0.8$.

$12\ \mathrm{cm}^{-1}$ and $\mathrm{k}_\theta = 22\ \mathrm{cm}^{-1}$, in the two experiments the periodic modulation of turbulence is easily observed.

Notably, the measured frequency $f = \frac{\omega}{2\pi} = \mathrm{u}_\theta k_\theta / 2\pi$ proportional to the fluctuation velocity u_θ

$$u_\theta = v_{ph} + v_{E\times B} \quad (6)$$

where v_{ph} is turbulence phase velocity in poloidal and $v_{E\times B}$ is plasma $\boldsymbol{E_r} \times \boldsymbol{B}$ velocity.

Researches on several tokamaks and stellerators in various plasma conditions have shown that the fluctuation velocity is often dominated by the $E \times B$ term [27,28,29,30,31]. But the hypothesis of negligible phase velocity is not completely trivial in some cases, especially in the confinement mode transition [25] and in ohmic confinement with low injected torque [32,33]. In the case of drift waves, the phase velocity is proportional to the diamagnetic drift frequency in the stationary plasma [27]. As there is no significant correlation

between the measured poloidal rotation velocity and the diamagnetic drift frequency, we can exclude a direct influence of the drift wave phase velocity on the poloidal rotation. The velocity can be roughly calculated from the measured frequency

$$v_{E\times B} \approx 2\pi f/k \quad (7)$$

The frequency f is represented by $\langle f \rangle$ and can be estimated by the instantaneous time-varying frequency method [34,35],

$$\langle f \rangle \approx \frac{\sum_f f \cdot S_k(t,f)}{\sum S_k(t,f)} \quad (8)$$

where $S_k(t,f)$ is the spectrogram of turbulence at wave number **k**, and the integrated power of turbulence at **k** can be calculated by $S_k(t) = \sum S_k(t,f)$.

Some researches about poloidal velocity have been carried out with the diagnostics during the steady-state discharges [31,36].

3. Turbulence Modulation and Density Peaking

Two repeatable shots (80742, 80744) are selected for analysis. And there is no sawtooth during the phase we analyzed and the discharge was stable throughout the time. We can assume that both systems are in equilibrium at the initial moment, which will be used in the following analysis. Turbulence power, poloidal rotation speed and the plasma density peaking factor in the core plasma ($\langle n_e(0)\rangle / \langle n_e(0.5)\rangle$, $\langle n_e(\rho)\rangle$ is the line integrated density at $\rho = \frac{Z}{a}$, provided by POINT system in EAST [37]) are presented in figure 5. Electron density normalized to the central density, are shown in figure 6. The density profile sharps vary inside $\rho = 0 - 0.5$ is clear, which is relate to the deposition location of ECRH power. The analysis mainly focuses on the evolution of core parameters, while the mean poloidal rotation velocity $\rho = 0.4 - 0.8$ is shown in figure 5(b) and figure 5(e) for comparison.

In ECRH power modulation experiment with NBI, the higher ECRH power not only increases the intensity of the electron-scale turbulence, but also cause a reduction in the poloidal rotation speed. The core peaking factor decrease in the phase. The more serious electron-scale turbulence and weakened plasma flow may enhance turbulent transport, which raises the outward thermo-diffusive pinch and lead to the reduced peaking factor. In the stable discharge, the development of turbulence and plasma flow are the result of competition for free energy and decorrelation process, the details are shown in section 4. When the ECRH power drops, all the mechanisms are reversed and result in a enhancement in core density peaking. Changed ECRH power are followed by a process in which density peaking evolves toward an intermediate value, which is nonlinear and shown in figure 5(c). Under this experimental parameter, the distribution of free energy between the turbulence and the plasma flow may be comparable and competitive. When deviating from the

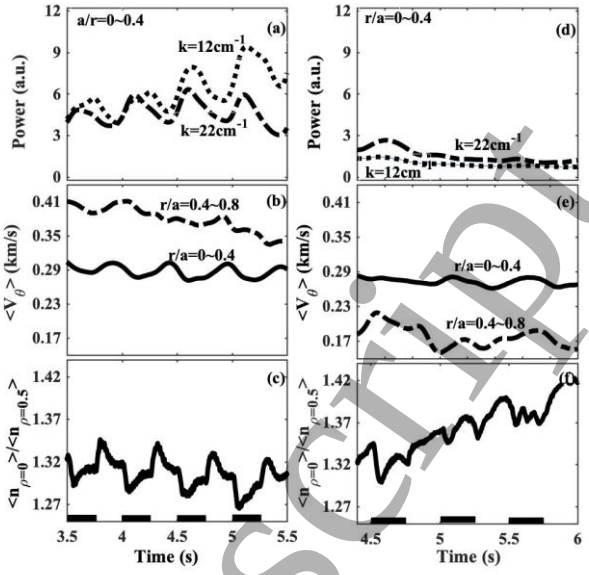

Figure 5. Time evolution of (a) and (d) turbulence intensity, (b) and (e) mean poloidal rotation velocity, (c) and (f) density profile peaking. Data in (a), (b) and (c) are from shot 80744, stable discharge in ECRH power modulation with NBI. Data in (d), (e) and (f) are from shot 80742, stable discharge in ECRH power modulation without NBI. The phases with higher ECRH power at 1.0 MW are marked by black rectangular frames in (c) and (f), and the ECRH power in the remaining

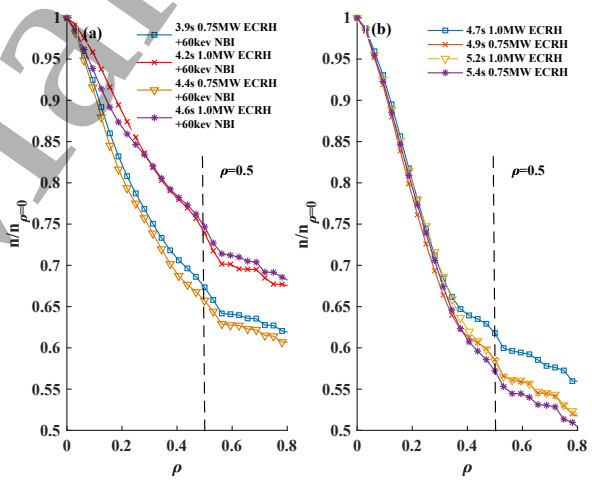

Figure 6. The electron density data are normalized to the central density. (a) the normalized density profile in ECRH power modulation experiment with NBI (shot 80744). (b) normalized density profile in the ECRH power modulation experiment without NBI (shot 80742).

equilibrium state, the distribution of free energy between the two may be changed.

In the ECRH power modulation experiment with NBI, core density peaking is effectively adjusted. Core density peaking factor is in the region 1.26-1.32 (figure 5(c)), and the modulation occurs in the core $\rho = 0 - 0.5$ (figure 6(a)). In the high performance fusion plasmas with high temperatures and low collisionality, electron-scale turbulence (ETG, TEM) can be coupled with MHD [26]. As the flat density gradient in the region $\rho = 0.5 - 0.8$ (figure 6 (a)) will not dramatically worsen the turbulence that driven by free energy,

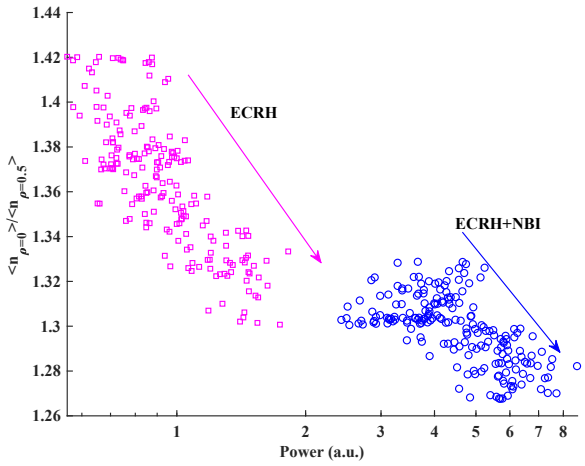

Figure 7. Density profile peaking factor in plasma core vs integrated turbulence intensity at $k = 12\text{cm}^{-1}$. Different squares and rings represent the turbulence intensity and core density peak factor at different moments, which are selected every 8 ms in shot 80742 and shot 80744 respectively.

the coupling between turbulence and MHD in the region may not be exacerbated. In a burning plasma, the inner high-temperature core where fusion reactions occur is closely related to the fusion energy gain. Effectively adjusting the density in the region $(\rho = 0 - 0.5)$ should be a way to control the fusion reaction. So the way we have found to modify core density profile peaking may be significant for the safely control of core fusion reactivity in future reactor.

The potential associations between turbulence intensity at $k_\theta = 12\ \text{cm}^{-1}$ and core density peaking factor in shot 80742 and shot 80744 are shown in Figure 7. The confinement moments selected satisfy $k_\theta \rho_s \sim 1.4 - 2.0$. The figure shows the slight enhancement of turbulence intensity in ECRH power modulation without NBI accompanied by a rapid peaking factor reduction. However, slightly change of the peaking factor in ECRH power modulation with NBI need a larger turbulence power at $k_\theta = 12\ \text{cm}^{-1}$. The intensity of turbulence and density peaking factor show a negative correlation. This result suggests that it may be feasible to adjust peaking factor by modifying turbulence intensity in future reactor with serious electron-scale turbulence, and the precise modulation of core density peaking need more research in future.

However, no effective measurement of core density peaking is found in ECRH power modulation without NBI, and the evolution of density peaking factor is different from that in ECRH power modulation with NBI (figure 5(c) and figure 5(f)). The detail divergence of density profile is shown in figure 6. The discharge with NBI injection and discharge without NBI injection are two different nonlinear systems. And NBI may be an important initial condition determining the plasma nonlinear system in ECRH power modulation experiments.

4. Turbulence and Poloidal Rotation

The self-organization of plasmas is an inherent mechanism, and manifests as holistic phenomena creating and sustaining this localized structure [38]. The relationship between the turbulence intensity and the peaked density is monitored experimentally, and the corresponding relationship between the turbulence intensity and the poloidal rotation (plasma flow) is also observed. Plasma flows in high-parameter plasma may be driven by a number of factors. In this lower-parameter plasma, some results are obtained based on experimental data. The results can not completely define the mechanism of plasma flows generation, and the unknown mechanisms may also exist, especially in high-parameter plasmas. This requires further research in theory and physics in the community of fusion.

4.1 Turbulence Gradient and Intrinsic Poloidal Rotation

In this section, the quasi-linear theory of turbulence driven rotation is used to explain a possible relationship between the electron-scale turbulence and the poloidal rotation. The poloidal momentum sources driven by turbulence includes poloidal Reynolds stress iteam $\langle n \rangle \langle \tilde{v}_r \tilde{v}_\theta \rangle$, convection item $\langle \tilde{v}_\theta \rangle \langle \tilde{v}_r \tilde{n} \rangle$ and the nonlinear term $\langle \tilde{v}_\theta \tilde{v}_r \tilde{n} \rangle$ [39]. The latter two can be neglected, when electrostatic turbulence is modulated and reviewed in a stable discharge. According to theadvective nonlinearity of the incompressible fluid momentum balance equation [11], the following conclusions can be drawn. The gradient in the turbulent Reynolds stress constitutes an intrinsic torque and as such functions of a momentum source,

$$\frac{\partial}{\partial t}\langle V_\theta \rangle = -\langle \frac{\partial}{\partial r}\left(\tilde{V}_r \tilde{V}_\theta\right)\rangle = -\int dm|k_\theta|\frac{\hat{s}}{q}\int dx \frac{\partial}{\partial r}\left(\tilde{V}_{r_k}^* \tilde{V}_{\theta_k}^*\right) \quad (9)$$

It indicates the variation of Reynolds stress in the radial is necessary for poloidal rotation, and the variation is generated by the radial divergence of turbulence spectrum.

The quasi-linear theory of turbulence driven rotation shows that the divergence of wave energy density flow is a necessary condition for driving the average poloidal rotation. The electron-scale turbulence is perpendicular to the magnetic lines of force and propagates in the radial direction. The properties of the locally heating electrons of ECRH inevitably lead to asymmetry of the turbulent spectrum in the radial direction. This divergence between the Reynolds pressure and the radial electric field-driven Lorentz force generated by the turbulence is balanced, since

$$F \sim -\frac{J_r B_t}{c} \quad (10)$$

The total radial current contributed by electron-scale turbulence and ion-scale turbulence can be described using Poynting theory. This yields [6]

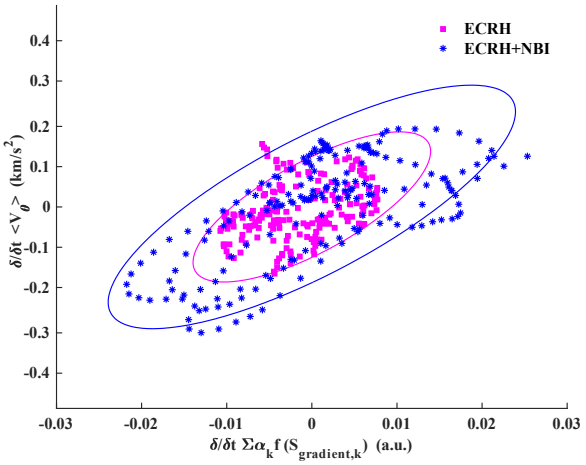

Figure 8. Scatter plot of $\partial/\partial t\langle V_\theta\rangle$ versus the time derivative of electron-scale turbulence driven rotation $\partial/\partial t\sum_{k_1,k_2}\alpha_k f(S_{gradient,k})$.

$$J_r = \sum_k \frac{ck_\theta}{B_0}(2\omega_k)^{-1}\frac{\partial S_{k,r}}{\partial r} \quad (11)$$

where the $S_{k,r}$ is the energy density flux of drift turbulence. It is assumed that the neoclassical magnetic pump resistance balances the turbulent drive due to the quasi-linear force, so the poloidal speed is [39]

$$V_\theta \approx \frac{F}{\mu m_i n_0} \quad (12)$$

where $\mu = qv_{thi}/R$. When the magnetic topology is not changed, the ratio of electron-scale turbulence intensities at different at different radial locations can roughly describe the contribution $f(S_{gradient})$ to the poloidal rotation speed

$$\langle V_\theta\rangle \propto \sum_{n=1}^{n}\alpha_{k_n} f(S_{gradient,k_n}) \quad (13)$$

$$f(S_{gradient,k}) = \frac{k(2\omega_k)^{-1}}{L_n m_i n_0}\frac{\nabla S_{k,r}}{\nabla r} \quad (14)$$

where α_k is coefficient or weight range from -1 to 1 and $\sum|\alpha_k| = 1$, k_n is the representative wave number of electron-scale turbulence. In the experiment, two representative wave numbers are chosen ($n = 2$, $k_1 = 12\ cm^{-1}$ and $k_2 = 22\ cm^{-1}$). The intensites of the turbulence ($S_{k=12\ cm^{-1}}$, $S_{k=22\ cm^{-1}}$) in two radial regions (core $\rho = 0-0.4$, outer $\rho = 0.4-0.8$) are measured simultaneously by the CO_2 laser collective scattering diagnostics in EAST tokamak. During the steady discharge, the frequency of the turbulence ω_k under fixed scale is assumed to be constant, and the effect of turbulent phase velocity on the calculation of core poloidal speed is negligible [31]. The mean poloidal rotation speed in the core is emploied to described the change of $\langle V_\theta\rangle$. The density of electron in the caculation is provided by POINT system in EAST.

Scan the coefficient α_{k_n} to make $\sum_{n=1}^{n}\alpha_{k_n} f(S_{gradient,k_n})$ and velocity similar in the period, and then calculate the time derivatives of the them. After that, data of $\partial/\partial t\langle V_\theta\rangle$ and $\partial/\partial t\sum_{k_1,k_2}\alpha_k f(S_{gradient,k})$ from shot 80742 and shot 80744 are selected every 8 ms and marked in figure 8. It is worth noting that since the turbulence intensity measured by the system is not the absolute value, eventually only relative values are obtained in the team $\partial/\partial t\sum_{k_1,k_2}\alpha_k f(S_{gradient,k})$. In electron-scale turbulence modulation experiments, the poloidal rotation acceleration $\partial/\partial t\langle V_\theta\rangle$ versus the time derivative of electron- scale turbulence gradient $\partial/\partial t\sum_{k_1,k_2}\alpha_k f(S_{gradient,k})$ is shown in figure 5. In ECRH power modulation without NBI, scanning the contribution coefficient of electron turbulence at different scale, when 40% comes from turbulence at $k_\theta = 22\ cm^{-1}$ and 60% comes from turbulence at $k_\theta = 12\ cm^{-1}$ ($\alpha_{k=22cm^{-1}} = 0.4$, $\alpha_{k=12cm^{-1}} = 0.6$) , $\sum_{k_1,k_2}\alpha_k f(S_{gradient,k})$ is similar with the trend of poloidal rotation. In ECRH power modulation with NBI, $\alpha_{k=12cm^{-1}} \approx -1$ and $\alpha_{k=22cm^{-1}} \approx 0$.

In figure 8, we find that the acceleration of mean poloidal rotation speed (equivalently, Reynolds stress gradient $\frac{\partial}{\partial t}\langle V_\theta\rangle = \langle -\partial/\partial r(\widetilde{V}_r\widetilde{V}_\theta)\rangle$ is close to linearly with $\partial/\partial t\sum_{k_1,k_2}\alpha_k f(S_{gradient,k})$, and $\partial/\partial t\sum_{k_1,k_2}\alpha_k f(S_{gradient,k})$ is dominated by the gradient of electron-scale turbulence energy density flux in stable discharge. In the two shots with stable discharges, the exprimental results show a similar characteristic to the quasi-linear theory of turbulence driven rotation, the electron-scale turbulence may modulate the poloidal rotation via Reynolds stress. The opposite effect of electron-scale turbulence driven poloidal rotation (α_k changes sign) in presence or absence of NBI may due to the difference of turbulence characteristic.

Residual Reynolds stress can drive the mean flow and zonal flow [4,7,8]. The correlation spectrum of the poloidal velocity at different radial positions ($\rho = 0-0.4$ and $\rho = 0.4-0.8$) showed in figure 9. According to the empirical formula [40], the frequency of geodesic acoustic modes (GAMs) [41] under this experimental condition is 20-25 kHz, which is consistent with the radially strongly correlated perturbation structure at 20kHz. Except for the 2kHz fluctuation, no disturbance was found at 20kHz in the magnetic field measurement signals. Therefore, we conclude that GAM exists during the experiment. The fact that GAM decays rapidly as it propagates inward is clarified [42], which is also observed in the core poloidal speed power spectrum with a small intensity peak (figure 10). And the intensity of GAM does not change significantly in the phase we interested. In figure 10, strong fluctuations occur at low frequencies of $\langle V_\theta\rangle$, and the power of fluctuations decreases rapidly with increasing frequency. The fluctuations may related to the potential, and a similar distribution of fluctuation power is also observed in the potential measurement [43].

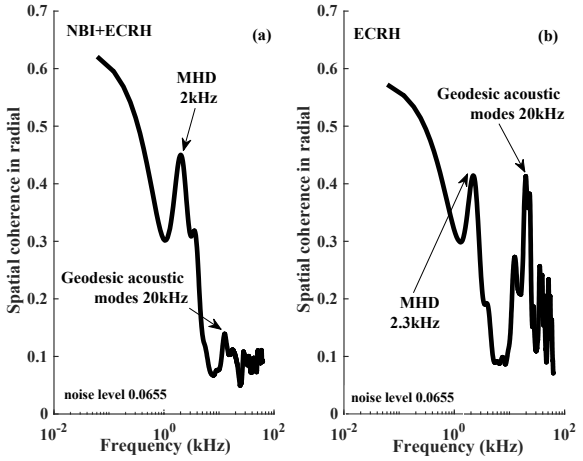

Figure 9. The spatial correlation of poloidal rotational speed $\langle V_\theta \rangle$ at two regions $\rho = 0 - 0.4$ and $\rho = 0.4 - 0.8$. (a) ECRH power modulation experiment with NBI (shot 80744), (b) ECRH power modulation experiment without NBI (shot 80742).

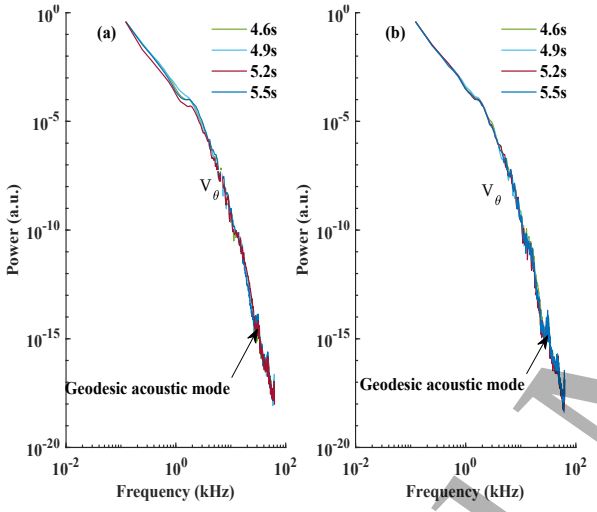

Figure 10. The power spectrum poloidal rotational speed $\langle V_\theta \rangle$. (a) ECRH power modulation experiment with NBI (shot 80744), (b) ECRH power modulation experiment without NBI (shot 80742).

In stable discharge phase with ECRH power modulation and constant NBI injection (shot 80744), turbulence may modulate the plasma flows via Reynolds stress in plasma core, and the plasma flows may exhaust the free energy of turbulence and influence the core density peaking associated with fluctuation amplitude. The modulation of the density peaking factor may be the final result of a complex self-organizing process. Unfortunately, we cannot be sure that zonal flow or/and mean flow play the decisive role in the density peaking factor modulation process. And we do not rule out other unknown mechanisms.

4.2 Flow Shear and Turbulence Coherence

Radial divergence of turbulence energy density provides torque for poloidal rotation, while the flow shearing rate $\omega_{shear} = \left|\frac{\partial \langle V_\theta \rangle}{\partial r}\right|$ can change turbulence structure through a

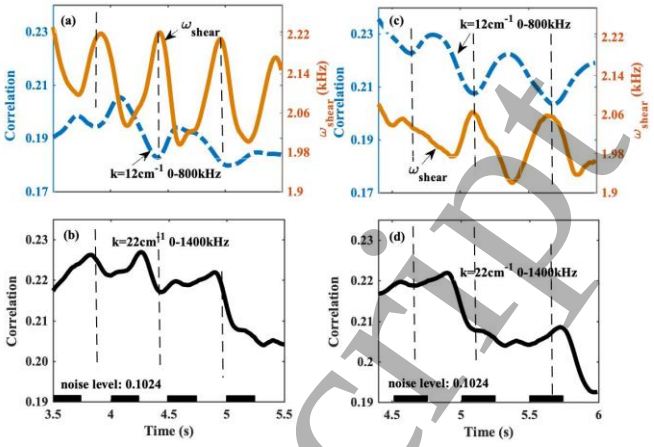

Figure 11. Time evolution of turbulence spatial cross-correlation between $\rho = 0 - 0.4$ and $\rho = 0.4 - 0.8$. Flow shearing rate is supplemented in (a) and (c) for comparison. (a) k = 12cm^{-1}, (b) k = 22cm^{-1} in ECRH power modulation experiment with NBI (shot 80744). (c) k = 12cm^{-1}, (d) k = 22cm^{-1} in ECRH power modulation experiment without NBI (shot 80742). The phases with higher ECRH power at 1.0 MW are marked by black rectangular frames in (b) and (d), and the ECRH power in the remaining phases is 0.75MW.

decorrelation process [44]. The relationship between the spatial cross-correlation of turbulence ($k_\theta = 12\ cm^{-1}$ and $k_\theta = 22\ cm^{-1}$) and flow shearing rate is shown in figure 11.

Spatial cross-correlation spectrum of turbulence reflects the characteristics of turbulent structure [45]. In shot 80742 and shot 80744, the spatial cross-correlation of turbulence at $k_\theta = 12\ cm^{-1}$ is prominent in the frequency band 0-800kHz, and the range is expanded to 0-1400kHz at $k_\theta = 22\ cm^{-1}$. There is a negative correlation between the poloidal flow shearing rate ω_{shear} and the spatial correlation of turbulence at $k_\theta = 12\ cm^{-1}$ (figure 11(a) and figure 11(c)). But this relationship does not exist at $k_\theta = 22\ cm^{-1}$ (figure 11(b) and figure 11(d)). The turbulent structure at $k_\theta = 22\ cm^{-1}$ may be not sensitive to the plasma flow shear. By comparing figure 11(a) and figure 5(c), we find that in ECRH power modulation experiment with NBI the trend of turbulent spatial correlation at $k_\theta = 12\ cm^{-1}$ and the trend of density peaking factor are opposite. And there is no significant correlation between density peaking factor and turbulent spatial correlation in ECRH power modulation experiment without NBI (figure 11(c), figure 5(f)). Therefore, the density peaking factor modulation based on the interaction between turbulence and flow requires certain conditions. And the result may be helpful in studying the relationship between decorrelation and transport.

5. Sawtooth and Density Peaking

Particle transport in magnetically confined plasma involves convection caused by various magnetic fluid activities, as well as anomalous transport caused by turbulence. For the primary role of the plasma density

profile, in addition to the magnetic fluid activity in the active region of the magnetic fluid, the usually transport zone is primarily anomalous transport.

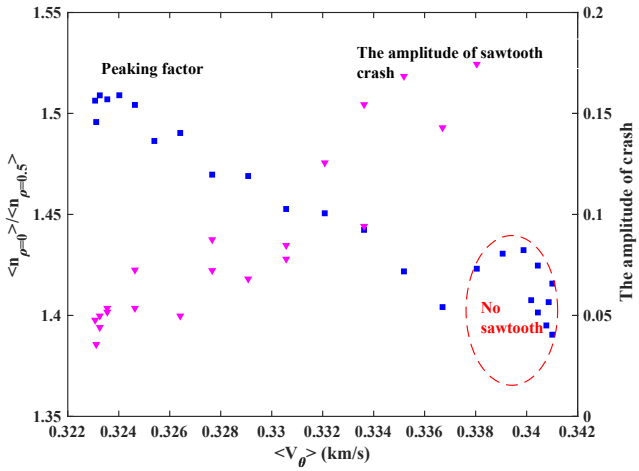

Figure 12. Shot 80733, core density profile peaking factor (blue) and the amplitude of sawtooth crash (red, assess with soft-X ray from position of sawtooth occur) versus core poloidal rotation speed.

The presence of sawtooth activity can influence density peaking in discharges with pumpout [46], but the density peaking shown in above chapters is affected by turbulence instead of sawtooth. Figure 12 shows the correlation between plasma flow, density peaking and sawtooth crash amplitude ($\frac{I_1-I_0}{I_0}$. I_0 and I_1 is the radiation intensity of soft x-ray before and after the sawtooth crash at the position where sawtooth occurs). We find that the greater the amplitude of sawtooth crash, the lower the core density peaking factor. The activity of sawtooth may have a greater impact on density peaking. And relationship between the poloidal rotation and sawtooth crash amplitude may imply a complex free energy distribution when multiple factors work together. But the underlying mechanism including the coupling of turbulence and MHD requires further research, and some basic works have been carried out [26].

6. Summary

In ECRH power modulation experiment with a constant NBI injection, we presented a study of core density peaking factor modulation. The core density peaking factor ($\rho = 0 - 0.5$) is well modulated from 1.26 to 1.32. In lower ECRH power pulse, higher poloidal rotation velocity and the lower electron-scale turbulence intensity are seen simultaneously, which is accompanied by a larger core density peaking factor. Opposite phenomenon occur in the higher ECRH power pulse. Larger turbulence changes at stronger intensity allow fine peaking factor modulation. Besides, the density gradient in the region $\rho = 0.5 - 0.8$ is unchanged. The results imply that this method of density peaking modulation may be suitable for future fusion reactors with severe turbulence and may not increase the danger of high-n MHD crash that driven by free energy.

The competition of plasma flow for free energy and the development of turbulence spatial structure are studied. We found that the correlations between turbulence and plasma flow may be responsible for the modulation of density peaking factor in the certain conditions. Besides, no effective adjustment of core density peaking is found in the ECRH power modulation experiment without NBI injection, which implies a different nonlinear physical system. The main experiments are carried out without sawtooth. And the effects of sawtooth on density peaking are also discussed at last.

Results suggesting the interactions between turbulence and plasma flow are self-organized behaviors, which may shed light on the understanding of the nonlinear system of magnetically confined plasma and providing a possible idea for controlling the fusion reactions rate. More work is still needed to study the mechanisms that affect the development of nonlinear systems and effectively control the peaking factor of core density.

Acknowledgements

Work supported by National Natural Science Foundation of China under Grand Nos. 11475222, 11275232,11575238.

References

[1] Wang X., Mordijck S., Doyle E. J., Zeng L., Staebler G.M., Meneghini O. and Smith S.P. 2018 *Nucl. Fusion* **58** 016025
[2] Valovic M. et al 2002 *Plasma Phys. Control. Fusion* **44** 1911
[3] Weisen H. et al 2005 *Nucl. Fusion* **45** L1
[4] Garbet X., Garzotti L., Mantica P., Nordman H., Valovic M., Weisen H. and Angioni C. 2003 *Phys. Rev. Lett* **91** 035001
[5] Fable E., Angioni C. and Sauter O. 2010 *Plasma Phys. Control. Fusion* **52** 015007
[6] Hoang G.T. et al 2003 *Phys. Rev. Lett.* **90** 155002
[7] Angioni C., Peeters A. G., Pereverzev G. V., Ryter F. and Tardini G. 2003 *Phys. Rev. Lett.* **90** 205003
[8] Angioni C. Peeters A. G., Pereverzev G. V., Ryter F., Tardini G. and ASDEX Upgrade Team 2003 *Phys. Plasmas* **10** 3225
[9] Yoshida M., Ide S., Takenaga H., Honda M., Urano H., Kobayashi T., Nakata M., Miyato N. and Kamada Y. 2013 *Nucl. Fusion* **53** 083022
[10] Angioni C., Peeters A.G., Garbet X., Manini A., Ryter F. and ASDEX Upgrade Team 2004 *Nucl. Fusion* **44** 827
[11] Ritz Ch. Roger P., Bengtson D., Levinson S. J. and Powers E. J. 1984 *Phys. Fluids* **27** 2956
[12] Moyer R. A. et al 1995 *Phys. Plasmas* **2** 2397
[13] Shats M. G. et al 2000 *Phys. Rev. Lett* **84** 6042
[14] Terry P. W., Newman D. E. and Ware A. S. 2001 *Phys. Rev. Lett* **87** 185001
[15] Diamond P. H. and Kim Y.-B. 1991 *Phys. Plasmas* **3** 1626
[16] Horton W. 1999 *Rev. Mod. Phys* **71** 735
[17] Diamond P. H., Itoh S-I., Itoh K. and Hahm T. S. 2005 *Plasma Phys. Control. Fusion* **47** R35

[18] Itoh K., Itoh S.-I., Diamond P. H., Hahm T. S., Fujisawa A., Tynan G. R., Yagi M. and Nagashima Y. 2002 *Phys. Plasmas* **13** 055502
[19] McDevitt J. and Gürcan Ö. D. 2012 *Phys. Plasmas* **19** 102311
[20] Peeters A.G. et al 2005 *Nucl. Fusion* **45** 1140
[21] Rhodes T. L. et al 2007 *Phys. Plasmas* **14** 056117
[22] Xu H. D. et al 2016 *Plasma Sci. Technol.* **18** 442
[23] Cao G. M. Li Y. D., X Q. Li,. Zhang D., Sun P. J., Wu G. J., and Hu L. Q., and the EAST Team 2015 *Phys. Scr.* **90** 025603
[24] Mazzucato E. 2006 *Plasma Phys. Control. Fusion* **48** 1749
[25] Bi J., Li Y. D., Wu G. J., Li P., Sun P. J., Lan T., Wang S. X., Zhao H. L. and the EAST Team1 2019 *Plasma Phys. Control. Fusion* **61** 065011
[26] Sun P.J. et al 2018 *Nucl. Fusion* **58** 016003
[27] Hirsch M., Holzhauer E., Baldzuhn J., Kurzan B. and Scott B. 2001 *Plasma Phys. Control. Fusion* **43** 1641-1660
[28] Conway G. D., Schirmer J., Klenge S., Suttrop W., Holzhauer E. and the ASDEX Upgrade Team 2004 *Plasma Phys. Control. Fusion* **46** 951-970
[29] Schirmer J., Conway G.D., Zohm H., Suttrop W. and the ASDEX Upgrade team 2006 *Nucl. Fusion* **46** S780
[30] Hennequin P., Honoré C., Truc A., Quéméneur A., Fenzi-Bonizec C., Bourdelle C., Garbet X., Hoang G.T. and the Tore Supra team 2006 *Nucl. Fusion* **46** S771-S779
[31] Shen H. G. et al 2015 *Nucl. Fusion* **55** 093004
[32] Lebschy A. et al 2018 *Nucl. Fusion* **58** 026013
[33] McDermott R.M., Angioni C., Conway G.D., Dux R., Fable E., Fischer R., Pütterich T., Ryter F., Viezzer E.and theASDEX Upgrade Team 2014 *Nucl. Fusion* **54** 043009
[34] Cohen L. 1989 *Proc. IEEE* **77** 941
[35] Yu C. et al 1992 *Nucl. Fusion* **32** 1545
[36] Zhang W. Y., Li Y. D., Zhang X. J., Lan T., Gao X., Liu Z. X., Sun P. J., Zhang X. D., Li J. and the HT-7 Teams 2012
[37] Qian J. P. et al 2017 *Nucl. Fusion* **57** 036008
[38] Nishiura M., Yoshida Z., Kenmochi N., Sugar T., Nakamura K., Mori T., Katsura S., Shirahata K. and Howarad J. 2019 *Nucl. Fusion* **59** 096005
[39] Wang L., Wen T. L. and Diamond P.H. 2016 *Nucl. Fusion* **56** 106017
[40] Ido T. et al 2006 *Plasma Phys. Control. Fusion* **48** S41
[41] Lan T. et al 2008 *Phys. Plasmas* **15** 056105
[42] Mckee G. R. Fonck R. J. and Jakubowski M. 2003 *Phys. Plasmas* **10** 1712
[43] Velasco J L. et al 2013 *Plasma Phys. Control. Fusion* ***55*** 124044
[44] Xu M. et al 2012 *Phys. Rev. Lett* **108** 245001
[45] Wu G. J., Li Y. D., Sun P. J., Li P., Bi J., Wang S. X., Liu H. Q., Zhang X. D., Hu L. Q. and EAST Team 2018 *Phys. Plasmas* **25** 082302
[46] Zabolotsky A., Weisen H. and TCV Team 2006 *Plasma Phys. Control. Fusion* **48** 369